SIRM 2015 – 11th International Conference on Vibrations in Rotating Machines,
Magdeburg, Deutschland, 23. – 25. February 2015

On the Numerical Simulation of Nonlinear Transient Behavior of Compliant Air Foil Bearings

Jon S. Larsen [1,2], **Bo B. Nielsen** [2], **Ilmar F. Santos** [2]

[1] Siemens A/S - Aeration Competence Center, 3000 Helsingør, Denmark
[2] Department of Mechanical Engineering, Technical University of Denmark, 2900 Kgs. Lyngby, Denmark

Abstract

Compliant Air Foil Bearings (AFB) have fundamental importance in the development of high speed machines due to low friction and no need of an external lubrication system, leading to a more environmental-friendly design. Nevertheless, rotors supported by such a type of bearing are more sensitive to unbalance and nonlinear instabilities due to low level of damping.

The transient nonlinear behaviour of rotors supported by AFBs demands the solution of the Reynolds equation for compressible fluid coupled to the compliance of top/bump foil surfaces and the friction between parts of this complex flexible structure. The nonlinear transient simulation of rotors interacting with AFB is still a challenge and a very time-consuming task. In the particular case of assuming the variation of pressure in time dp/dt negligible, time simulations for predicting rotor-bearing transient behaviour can be carried out relatively safely and without numerical instability problems. Nevertheless, a precise and correct way of dealing with the nonlinear problem is taking into consideration the variation of pressure in time, i.e. dp/dt. In this framework, this paper gives an original contribution by implementing a method, as proposed in the literature, in which the variation of pressure in time dp/dt is included as part of the state space variable domain. It is extended to simulate the transient and nonlinear behaviour of an industrial AFB, built by three independent segments and coupled to a rigid rotor as used in a Siemens compressor. An efficient finite element model previously developed, is used for the discretisation of the pressure field and foil compliant structure.

The theoretical results are validated against the literature and the importance of the term dp/dt is carefully elucidated. A parameter study with focus on the transient nonlinear behavior of the rotor-bearing system is carried out and the efficiency of the method presented is discussed, highlighting advantages and drawbacks.

Nomenclature

$(\ddot{\cdot})$	Time derivative, $\frac{\partial^2}{\partial \tau^2}$
$(\dot{\cdot})$	Time derivative, $\frac{\partial}{\partial \tau}$
$(\,)^*$	Approximating field
A, B	Bearings
C	Radial clearance
E	Modulus of elasticity of foil
L, $\tilde{L}$	Bearing length, $\tilde{L} = L/R$
N_p	Number of pads
R	Journal radius
S	Bearing number, $S = \frac{6\mu\omega}{p_a}\left(\frac{R}{C}\right)^2$
S^e	Element surface
S_b	Bump foil pitch
V	Volume
W	Static load
b, $\tilde{b}$	Structural damping per unit area, $\tilde{b} = \frac{C}{p_a \omega} b$
e, ε	Journal eccentricity components, $\varepsilon = e/C$
h, $\tilde{h}$	Film height, $\tilde{h} = h/C$
h_c, $\tilde{h_c}$	Film height correction, $\tilde{h_c} = h_c/C$
h_r, $\tilde{h_r}$	Film height (rigid), $\tilde{h_r} = h_r/C$
h_s, $\tilde{h_s}$	Slope height, $\tilde{h_s} = h_s/C$
k, $\tilde{k}$	Structural stiffness per unit area, $\tilde{k} = \frac{C}{p_a} k$
l_1	Distance to Bearing A
l_2	Distance to Bearing B
p, $\tilde{p}$	Film pressure, $\tilde{p} = p/p_a$
p_a	Ambient pressure
t_b	Thickness of bump foil
t_t	Thickness of top foil
u	Unbalance kg·m
x, y, z	Cartesian coordinates
CG	Center of gravity
η	Structural loss factor of foils
μ	Dynamic viscosity
$\nabla\cdot$	Divergence
∇	Gradient, $\nabla = \left\{\frac{\partial}{\partial\theta},\ \frac{\partial}{\partial\tilde{z}}\right\}$

ν Poisson's ratio of foil
ω Angular speed of journal
ψ Film state variable
θ Circumferential angle
θ_l First pad leading edge angle
θ_s First pad slope extend
θ_t First pad trailing edge angle
$\tilde{\theta}$ Circumferential coordinate, $\tilde{\theta} = \theta R$
ξ, η Gauss points
t, τ Time, $\tau = \omega t$
$\{F_{ub}\}, \{\tilde{F_{ub}}\}$ Unbalance force vector, $\{\tilde{F_{ub}}\} = \frac{1}{p_a R^2}\{F_{ub}\}$
$\{F\}, \{\tilde{F}\}$ Bearing force vector, $\{\tilde{F}\} = \frac{1}{p_a R^2}\{F\}$
$\{R\}$ Residual vector
$\{S\}$ Advection vector, $\{S\} = \{S,\ 0\}^T$
$\{W\}, \{\tilde{W}\}$ Load vector, $\{\tilde{W}\} = \frac{1}{p_a R^2}\{W\}$
$\{\psi\}$ Film state vector
$\{\mathbf{n}\}$ Unit normal vector
$\{\tilde{h}_c\}$ Foil deformation vector
$\{\tilde{h}\}$ Height vector
$\{\tilde{p}\}$ Pressure vector
$\{\varepsilon\}$ Eccentricity vector
$\{y\}$ State vector
$\{z_1\}, \{z_2\}$ Rotor state vectors
$[A]$ Fluidity matrix
$[B]$ Shape function derivatives matrix
$[G], [\tilde{G}]$ Gyroscopic matrix
$[M], [\tilde{M}]$ Mass matrix
$[N]$ Shape function matrix

1 Introduction

Gas bearings have been intensively investigated, theoretically as well as experimentally, for over five decades [3, 20, 21] although some initial publications are dated already from the beginning of last century [7]. In order to deal with time consuming rotor-bearing dynamic analysis in time domain, linear damping and stiffness coefficients were introduced to predict rotor-bearing stability [16]. The rapid development of computer science and increasing computer power, later enabled the solution of the mathematical models in time, and allowed for the inclusion of gas compressibility and foil compliance in the models. Although almost a century has passed since the first publications about gas bearings, the accurate time simulation of gas bearings with compliant surfaces is still a challenging and very time consuming task.

Prior to the presented work, different approaches for solving the compressible Reynolds equation has been investigated. Among others Wang and Chen [22] who used finite difference for the spatial and temporal dimensions when solving the Reynolds equation. They simulated the steady-state response of a perfectly balanced rigid rotor supported by two identical bearings. The spatial discretisation was performed with a central-difference scheme, while the temporal discretisation was performed with an implicit-backward-difference scheme. Furthermore, Successive Over Relaxation (SOR) was used in order to reduce the number of unknowns in the iteration step. Their solution took advantages of the bearings being rigid, hence only the rotor movement contributed to dh/dt. This made an explicit solution of the transient compressible Reynolds equation possible since a movement of the rotor resulted in a change in the gap and then a change in pressure, which then again affected the rotor.

Arghir *et al.* [2] presented a finite volume solution, where the pressure was implicitly integrated for a prescribed gap perturbation to calculate linear stiffness and damping coefficients dependent on the perturbation amplitude. In the procedure, the rotor was stationary in one direction, while the other was perturbed by a sinusoidal displacement $A\sin(\omega t)$. At each time step, the reaction forces from the air film was calculated, including dp/dt, and based on the displacement/velocity and reaction force pairs, the least square method was used to calculate the linear stiffness and damping for a given amplitude A. This allowed a linear analysis of a rotor system to take into account the nonlinearities related to the vibration amplitude of the rotor in the air bearings. This method works well for calculating the linear coefficients in a bearing with gap discontinuities e.g. thrust bearing.

Song and Daejong [19] calculated the time dependent pressure in the next time step by explicit time integration, but by utilising the present and previous time step values for the gap size. As stated in the paper, this was done to reduce the computational time spend in each time step, but this also required very small time steps in order to minimize the error introduced when dp/dt and dh/dt are taken from different time steps. Le Lez *et al.* [14] used a similar method to [19]. This method was also used in [23] to solve the transient Reynolds equation, but with four-node planar finite elements for the spatial discretisation of the Reynolds equation and for a rigid gas journal bearing. Lee *et al.* [15] also used a four-node finite element to solve the compressible Reynolds equation in time and space and a backward-difference iterative procedure to solve the pressure in time. This solution was used in conjunction with a finite element model of the bump foil, affected by coulomb friction at the bump foils contact points, to investigate the performance of a rigid rotor symmetrically supported by two bearings under different bearing configurations.

More recently Bonello and Pham [4, 18] solved the nonlinear Reynolds equation by using an alternative state variable $\psi = ph$. Using this alternative state variable, it was possible to solve the Reynolds equation explicitly with

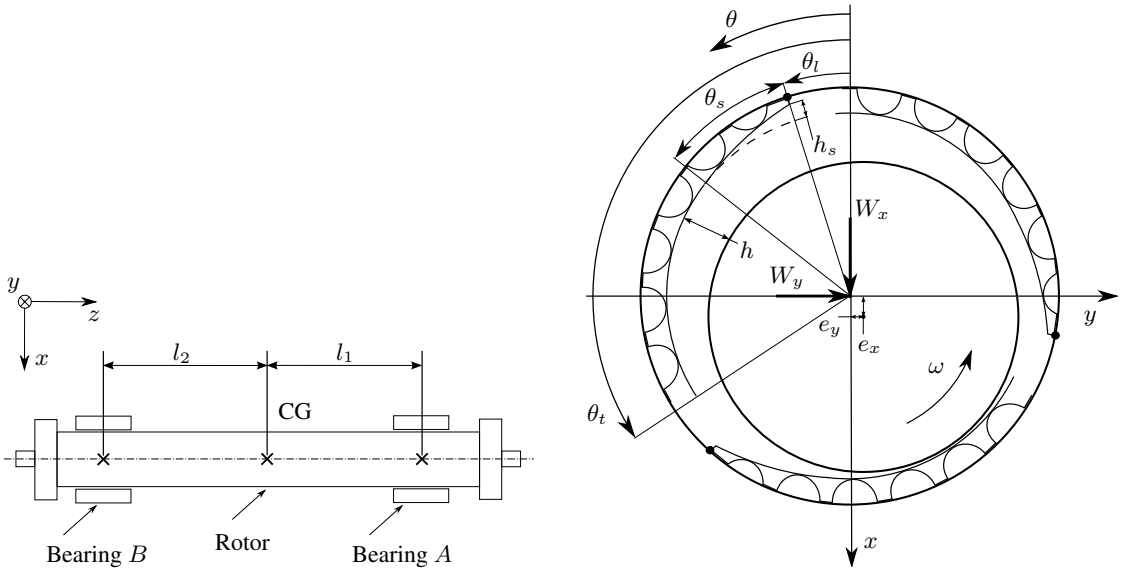

(a) Shaft and bearings.

(b) Detailed view of bearing geometry.

Figure 1: Schematics and nomenclature of a rigid rotor supported by foil journal bearings.

$d(ph)/dt$ calculated in the same time step. For spatial discretisation, a finite difference and Galerkin Reduction method were used. The solution for the transient compressible Reynolds equation was then coupled to the simple elastic foundation model, and the transient response of a rotor system was presented.

This paper is a continuation of the work done by the authors reported in [12], where the compressible Reynolds equation is solved for an equilibrium position and a perturbation method is used to obtain the linear stiffness and damping coefficients and perform rotor-bearing dynamic analyses. In this framework, this paper gives an original contribution to the time simulation of a rigid rotor supported by a set of industrial foil bearings. Bonello and Phams approach is used to properly solve the coupled equations of motion related to the time-dependent fluid film pressure and the rotor lateral movements. Instead of finite differences and Galerkin Reduction methods, the finite element method is used to evaluate the compressible Reynolds equation in time. The theoretical results are validated against the literature and the importance of the term dp/dt is carefully elucidated. A parameter study with focus on the transient nonlinear behaviour of the rotor-bearing system is carried out, and the efficiency of the method presented is discussed, highlighting advantages and drawbacks.

2 Mathematical model

In Fig. 1, the schematics of the rotor-bearing system is illustrated. With the nodal vector defined as $\{\varepsilon\} = \{\varepsilon_{Ax}, \varepsilon_{Ay}, \varepsilon_{Bx}, \varepsilon_{By}\}^T$ describing the instantaneous position of the shaft in the bearing locations A and B, and under the assumption; that the shaft is rigid and subjected to small rotations around x- and y-axis, its equations of motion can be written in dimensionless form as

$$[\tilde{M}]\{\ddot{\varepsilon}\} - [\tilde{G}]\{\dot{\varepsilon}\} = \{\tilde{W}\} - \{\tilde{F}\} + \{\tilde{F}_{ub}\}. \tag{1}$$

Here, the dimensionless mass and gyroscopic matrices, $[\tilde{M}]$ and $[\tilde{G}]$, are given in Appendix A, together with the mass unbalance vector $\{\tilde{F}_{ub}\}$. Furthermore, $\{\tilde{W}\}$ is the static load vector and $\{\tilde{F}\}^T = \{\{\tilde{F_A}\}^T, \{\tilde{F_B}\}^T\}^T$ is the reaction force vector stemming from the bearings. It is composed by the reactions from the bearings A and B, which are determined by integration of the fluid film pressure for each particular bearing as

$$\{\tilde{F}\} = \begin{Bmatrix} \tilde{F}_x \\ \tilde{F}_y \end{Bmatrix} = \int_0^{\tilde{L}} \int_0^{2\pi} (\tilde{p} - 1) \begin{Bmatrix} \cos(\theta) \\ \sin(\theta) \end{Bmatrix} d\theta d\tilde{z}. \tag{2}$$

The bearing pressures can be obtained by solving the Reynolds equation for compressible fluids for each bearing. This can be written dimensionless in vector form [6] as

$$\nabla \cdot \left(\tilde{p}\tilde{h}^3 \nabla \tilde{p}\right) = \nabla \cdot \left(\tilde{p}\tilde{h}\right) \{S\} + 2S \frac{\partial}{\partial \tau}\left(\tilde{p}\tilde{h}\right) \tag{3}$$

where the film height is defined as

$$\tilde{h}(\varepsilon_x, \varepsilon_y, \tilde{p}, \dot{\tilde{h}}_c) = \tilde{h}_r(\varepsilon_x, \varepsilon_y) + \tilde{h}_c(\tilde{p}, \dot{\tilde{h}}_c) \tag{4}$$

and $\tilde{h}_r(\varepsilon_x, \varepsilon_y)$ is the undeformed rigid height which depends of the rotor eccentricity and $\tilde{h}_c(\tilde{p}, \dot{\tilde{h}}_c)$ is a pressure dependent deformation in the foils referred to as the compliant height. For a bearing with the geometry as illustrated in Figure 1b and under the assumption of simple elastic foundation model [8, 9], expressions for these heights are given in Appendix B.

2.1 Solution strategy

The equations (1) through (4) constitutes the mathematical model for the rotor-bearing system. In order to simulate the nonlinear rotor response, a commonly used strategy is to rewrite (1) to a system of ODEs to be integrated while the bearing forces $\{\tilde{F}\}$ are updated at each time step. The bearing forces relates to the pressure, through (2), which is then obtained by solving (3). This can be accomplished by discretising the film PDE and substituting the time dependent terms by backward difference approximations as;

$$\frac{\partial\{\tilde{p}\}}{\partial \tau} \approx \frac{\{\tilde{p}\}_n - \{\tilde{p}\}_{n-1}}{\Delta\tau}, \quad \frac{\partial\{\tilde{h}\}}{\partial \tau} \approx \frac{\{\tilde{h}\}_n - \{\tilde{h}\}_{n-1}}{\Delta\tau}, \tag{5}$$

where n is the current time-step. The pressure can then be found by iteratively solving a set of nonlinear algebraic equations. Following the above described strategy, the time dependent terms are lagging behind in time since they are based on the previous time-step in the integration of the rotor ODEs. As pointed out by Bonello and Pham [4, 18], this method does not preserve the true simultaneously coupled nature of the state variables, $\varepsilon, \tilde{p}, \tilde{h}_c$, of the system. This means that very small time-steps are necessary in order to insure an accurate solution. It makes the solution slow, and being strictly rigorous, each simulation should be accompanied by a convergence study on the time-step size to ensure an accurate solution.

Another problem with the above described solution strategy is the numerical stability. This is particularly related to the term $\partial\{\tilde{p}\}/\partial\tau$ which tends to become dominant and sensitive to the accuracy of $\{\tilde{p}\}_n - \{\tilde{p}\}_{n-1}$ due to the division by the very small number $\Delta\tau$. Assuming the term negligible is no option, simulations performed by Olsen [17] clearly showed that discarding this term leads to significant errors.

Bonello and Pham [4, 18] introduced a basic strategy to solve for all the state variables simultaneously and an efficient solution method based on a Gallerkin Reduction method to significantly limit the number of state-variables. Here, only the basic strategy is followed, which implies setting up one coupled system of nonlinear ODEs of the state variables $\varepsilon, \psi, \tilde{h}_c$, where $\psi = \tilde{p}\tilde{h}$.

2.2 Reynolds equation - discretisation

We discretise the PDE (3) using a standard Bubnov-Galerkin FE procedure with implementation of an isoparametric element formulation [5]. Firstly we perform a partial substitution with ψ to obtain

$$\nabla \cdot \left(\tilde{p}\tilde{h}^3 \nabla \tilde{p}\right) - \nabla \cdot \left(\tilde{p}\tilde{h}\right) \{S\} - 2S \frac{\partial \psi}{\partial \tau} = 0 \tag{6}$$

secondly, approximating fields $\tilde{p}^* = [N]\{\tilde{p}^e\}$ and $\dot{\psi}^* = [N]\{\dot{\psi}^e\}$ over the elements are introduced, where $\{\tilde{p}^e\}$ is the nodal pressures, $\{\dot{\psi}^e\}$ is the nodal film state variable and $[N]$ is the shape function matrix. Thus the Galerkin residual equation for (6), on the element level, is

$$\int_{V^e} [N]^T \nabla \cdot \left(\tilde{p}^* \tilde{h}^3 \nabla \tilde{p}^*\right) dV - \int_{V^e} [N]^T \nabla \cdot \left(\tilde{p}^* \tilde{h}\right) \{S\} dV - 2S \int_{V^e} [N]^T \dot{\psi}^* dV = \{0\} \tag{7}$$

where V^e is the element volume. Applying Greens theorem on (7) yields

$$\begin{aligned} -\int_{V^e}[B]^T\left(\tilde{p}^*\tilde{h}^3\nabla\tilde{p}^*\right)dV+\int_{V^e}[B]^T\left(\tilde{p}^*\tilde{h}\right)\{S\}dV-2S\int_{V^e}[N]^T\dot{\psi}^*dV \\ +\int_{S^e}[N]^T\left(\tilde{p}^*\tilde{h}^3\nabla\tilde{p}^*\right)\{\mathbf{n}\}dS-\int_{S^e}[N]^T\left(\tilde{p}^*\tilde{h}\right)\{S\}\{\mathbf{n}\}dS=\{0\} \end{aligned} \tag{8}$$

where matrix $[B]^T=\left[[N,_\theta]^T,\ [N,_{\tilde{z}}]^T\right]$ contains the spatial derivatives of the shape functions and $\{\mathbf{n}\}$ is the outward pointing unit normal vector of surface element dS. Due to continuity conditions, the boundary integrals vanishes and (8) reduces to

$$-\int_{V^e}[B]^T\left(\tilde{p}^*\tilde{h}^3\nabla\tilde{p}^*\right)dV+\int_{V^e}[B]^T\left(\tilde{p}^*\tilde{h}\right)\{S\}dV-2S\int_{V^e}[N]^T\dot{\psi}^*dV=\{0\}. \tag{9}$$

The spatial derivatives of the approximating pressure field are $\tilde{p}^*,_i=[N,_i]\{\tilde{p}^e\}$ with $i=\theta,\tilde{z}$ or in vector form, $\nabla\{\tilde{p}^*\}=[B]\{\tilde{p}^e\}$. Inserting this into (9) gives

$$[A^e]\{\dot{\psi}^e\}=\{R^e\} \tag{10}$$

where

$$\begin{aligned} [A^e]&=2S\int_{V^e}[N]^T[N]dV \\ \{R^e\}&=-\int_{V^e}[B]^T\tilde{p}^*\tilde{h}^3[B]dV\{\tilde{p}^e\}+\int_{V^e}[B]^T\{S\}\tilde{h}[N]dV\{\tilde{p}^e\}. \end{aligned} \tag{11}$$

The element vectors and matrices are expanded to structure size by the usual element summation:

$$\{R\}=\sum_e\{R^e\};\quad\{\tilde{p}\}=\sum_e\{\tilde{p}^e\};\quad\{\dot{\psi}\}=\sum_e\{\dot{\psi}^e\} \tag{12}$$

where the volume integrals are numerically integrated using a quadrature rule [5]. The scalar field quantities $\tilde{p}^*$, $\tilde{h}$, are calculated in the respective Gauss points (ξ_i,η_j) by use of the interpolation functions as:

$$q(\xi_i,\eta_j)=[N(\xi_i,\eta_j)]\{q^e\} \tag{13}$$

where q and $\{q^e\}$ are the scalar field quantities and nodal vectors respectively. Note that the right hand side of (10) is denoted $\{R^e\}$. In fact, $\{R^e\}$ is the residual that needs to be minimized in order to find the static equilibrium of the journal. When performing certain simulations in the time domain, it is very handy to start the simulations from this static equilibrium position. An efficient method for minimizing $\{R^e\}$ is given in [12].

2.3 Coupled system of ODEs

With the film PDE discretised, a system of ODEs of the form $\{\dot{y}\}=\mathbf{f}(\tau,\{y\})$ can be set up, and solved for all state variables simultaneously. The state-vector is defined as

$$\{y\}^T=\{\{\psi_A\}^T,\ \{\psi_B\}^T,\ \{\tilde{h}_{cA}\}^T,\ \{\tilde{h}_{cB}\}^T,\ \{z_1\}^T,\ \{z_2\}^T\}^T. \tag{14}$$

The right hand side $\mathbf{f}$ consists of three different equations. For each of the bearings A,B the film state is calculated by:

$$\{\dot{\psi}\}=[A]^{-1}\{R\}. \tag{15}$$

Vectorizing the pad deflection given in (26), the pad deflection for each of the bearings A, B is calculated by:

$$\{\dot{\tilde{h}}_c\} = \left(\frac{\{\tilde{p}\} - 1}{\tilde{k}} - \{\tilde{h}_c\} \right) \frac{1}{\eta} \tag{16}$$

and finally, the rotor state variables $\{z_1\}$ = $\{\varepsilon\}$ and $\{z_2\}$ = $\{\dot{\varepsilon}\}$ are calculated by:

$$\begin{Bmatrix} \{\dot{z_1}\} \\ \{\dot{z_2}\} \end{Bmatrix} = \begin{bmatrix} [0] & [I] \\ [0] & [\tilde{M}]^{-1}[\tilde{G}] \end{bmatrix} \begin{Bmatrix} \{z_1\} \\ \{z_2\} \end{Bmatrix} + \begin{Bmatrix} \{0\} \\ [\tilde{M}]^{-1}(\{\tilde{W}\} - \{\tilde{F}\} + \{\tilde{F_{ub}}\}) \end{Bmatrix}. \tag{17}$$

In this work, the system of ODEs are solved using the 'lsoda' solver from the Fortran library ODEPACK [10]. This solver has an automatic time-step control and switches between dedicated solvers for stiff and non-stiff systems. To efficiently solve the ODEs, a program for the discretisation and solution of (15) is implemented in C using the sparse solver DGBESV from the LaPack library [1]. However, the solution is still time consuming, and it should be highlighted, that Bonello and Pham [4, 18] significantly improved the solution efficiency by implementing a Galerkin reduction method.

2.4 Boundary conditions

In dimensionless form, the edge boundary conditions for the bearings, as depicted in Fig. 1b, are:

$$\begin{aligned} \tilde{p}(\theta_l, \tilde{z}) = \tilde{p}(\theta_t, \tilde{z}) = 1 \\ \tilde{p}(\theta, \tilde{L}/2) = \tilde{p}(\theta, -\tilde{L}/2) = 1. \end{aligned} \tag{18}$$

To obey these conditions, it is necessary to evaluate the film state variable $\dot{\psi} = \dot{\tilde{p}}h + \dot{\tilde{h}}p$. On the pad edges, we know that $\tilde{p} = 1$ and is constant so $\dot{\tilde{p}} = 0$. This means, that when solving (15) to obtain the film state variable, the following boundary conditions must be imposed:

$$\begin{aligned} \dot{\psi}(\theta_l, \tilde{z}) = \dot{\psi}(\theta_t, \tilde{z}) = \dot{\tilde{h}}(\dot{\varepsilon}_x, \dot{\varepsilon}_y, \dot{\tilde{h}}_c) \\ \dot{\psi}(\theta, \tilde{L}/2) = \dot{\psi}(\theta, -\tilde{L}/2) = \dot{\tilde{h}}(\dot{\varepsilon}_x, \dot{\varepsilon}_y, \dot{\tilde{h}}_c) \end{aligned} \tag{19}$$

which is achieved by using standard FE procedure. Symmetry conditions can be achieved by neglecting (19) on one side, e.g. on $(\theta, \tilde{L}/2)$. In this case, the reaction forces needs to be multiplied by two. A commonly used boundary condition [12], which is also used in this work, is to assume that the bearing foils deforms evenly over the length $\tilde{L}$ of the bearing. This condition is implemented by replacing $\{\tilde{p}\}$ in (16) by $\{\tilde{p}\}_m$, where $\{\tilde{p}\}_m$ is the arithmetic mean pressure over the length $\tilde{L}$.

In gas bearings, significant sub-ambient pressures may arise. These sub-ambient pressures can cause the top foil to separate from the bumps into a position in which the pressure on both sides of the pad are equalized. Heshmat [9] introduced a set of boundary conditions accounting for this separation effect. However, in this work, a simple Gümbel [6] boundary condition is imposed, which means that sub-ambient pressures are discarded when integrating the pressure (2) to obtain the bearing force components (W_x, W_y), essentially leaving the sub-ambient regions ineffective.

3 Results

As mentioned, the integration of (1) using a decoupled solution strategy, in which the time dependent terms of the Reynolds equation are approximated by backward difference approximations, can lead to numerical instability [17]. This problem is specifically related to the term dp/dt, hence it is interesting to investigate the significance of this term, in order to determine if it can be neglected in the simulations of the nonlinear rotor response.

Table 1: Geometry, material properties and operating conditions of a single pad foil bearing.

Parameters	Values	Parameters	Values
Bearing radius, R	19.05 mm	Young's modulus of bump foil, E	2.07×10^{11} Pa
Bearing length, L	38.10 mm	Poisson's ratio of bump foil, ν	0.3
Bearing clearance, C	32 μm	Loss factor, η	0.25
Bump foil thickness, t_b	0.1016 mm	Ambient pressure, P_a	1×10^5 Pa
Top foil thickness, t_t	0.2032 mm	Air viscosity, μ	1.95×10^{-5} Pa·s
Bump foil pitch, S_b	4.572 mm	Load, (W_x, W_y)	$(30, 0)$ N
Bump half length, l_0	1.778 mm	Speed, ω	$12,000$ RPM

Table 2: Geometry, material properties and operating conditions of the Siemens foil bearing test-rig

Parameters	Values	Parameters	Values
Bearing radius, R	33.50 mm	Bump foil height, h_b	0.9 mm
Bearing length, L	53.00 mm	Young's modulus of bump foil, E	2.07×10^{11} Pa
Bearing radial clearance, C	40 μm	Poisson's ratio of bump foil, ν	0.3
Number of pads, N_p	3	Foil friction coefficient, μ_f	0.2
First pad leading edge, θ_l	30 deg	Ambient pressure, p_a	1×10^5 Pa
First pad trailing edge, θ_t	145 deg	Air viscosity, μ	1.95×10^{-5} Pa·s
Slope extend, θ_s	30 deg	l_1	201.1 mm
Slope, h_s	50 μm	l_2	197.9 mm
Bump foil thickness, t_b	0.127 mm	$m = m_x = m_y$	21.1166 kg
Top foil thickness, t_t	0.254 mm	$I_{xx} = I_{yy}$	$525.166 \cdot 10^{-3}$ kgm^2
Bump foil pitch, S_b	7.00 mm	I_{zz}	$30.079 \cdot 10^{-3}$ kgm^2
Bump foil half length, l_0	3.30 mm		

3.1 Significance of dp/dt

To investigate the significance of the term dp/dt, a well known bearing geometry from the literature is simulated. Only a single bearing and a journal with two degrees of freedom are considered. The bearing geometry and operation conditions are listed in Tab. 1. The simulation is started at constant speed with the initial conditions $\{\varepsilon\} = \{\dot{\varepsilon}\} = \{0\}$, which in physical terms, corresponds to dropping the rotor from the center of the bearing. The result of this simulation is illustrated in Fig. 2. It is clear, that the two different solution strategies yields different results. Both yield the same equilibrium positions, but their transient trajectories toward this are different. Judging from the transient orbits, the journal-bearing system is less damped when including the term dp/dt. From Fig. 2, it is also seen that the calculations including the term dp/dt yields good agreement with similar results obtained by Pham and Bonello [4, 18]. The lower part of the trajectories coincide very well, but a slight discrepancy in the upper part is observed. This discrepancy could be due to different boundary conditions. For instance, a periodic boundary condition in the top of the bearing would cause the journal to lift higher on its way up, as found by Pham and Bonello [18].

3.2 Coupled rotor-bearing system

The rigid rotor-bearing system investigated in this paper (Fig. 1) is that of a test-rig designed for the identification of the linear bearing coefficients [11]. All parameters, operating conditions and dimensions are listed in Tab. 2. The authors wish to highlight, and reproduce by simulation, a phenomenon commonly seen when performing factory approval tests of compressors supported by AFBs. Specifically, the 'destabilizing effect' of rotor unbalance. First a perfectly balanced rotor, $\{F_{ub}\} = \{0\}$, is simulated at a variety of rotor speeds when dropped from the bearing centre i.e. $\{\varepsilon\} = \{\dot{\varepsilon}\} = \{0\}$. For these simulations, a foil stiffness of $k = 9.26$ GN/m^3 is used which is based on a structural finite element calculation of the foils [13] under the assumption of $\mu = 0.2$. At 30,000 RPM, the system is clearly unstable as illustrated in Fig. 3. At approximately 24,000 RPM, the system is marginally stable, and at 20,000 RPM the system is stable and quickly approaching its static equilibrium position as illustrated in Fig. 4. With the knowledge, that the perfectly balanced rotor-bearing system is stable at 20,000 RPM, a simulation with a different amount of unbalance applied is then performed. In Fig. 5, the orbit for bearing A and the associated frequency spectra for the two directions is illustrated with a rotor unbalance of $20\ \mathrm{g} \cdot \mathrm{mm}$ applied in each bearing 180 deg. out of phase. It is clear that the rotor-bearing system is still stable, moving in an almost circular orbit with the rotor running frequency (333 Hz).

Increasing the unbalance in each bearing to $40\ \mathrm{g} \cdot \mathrm{mm}$, an increase in the synchronous vibration components is

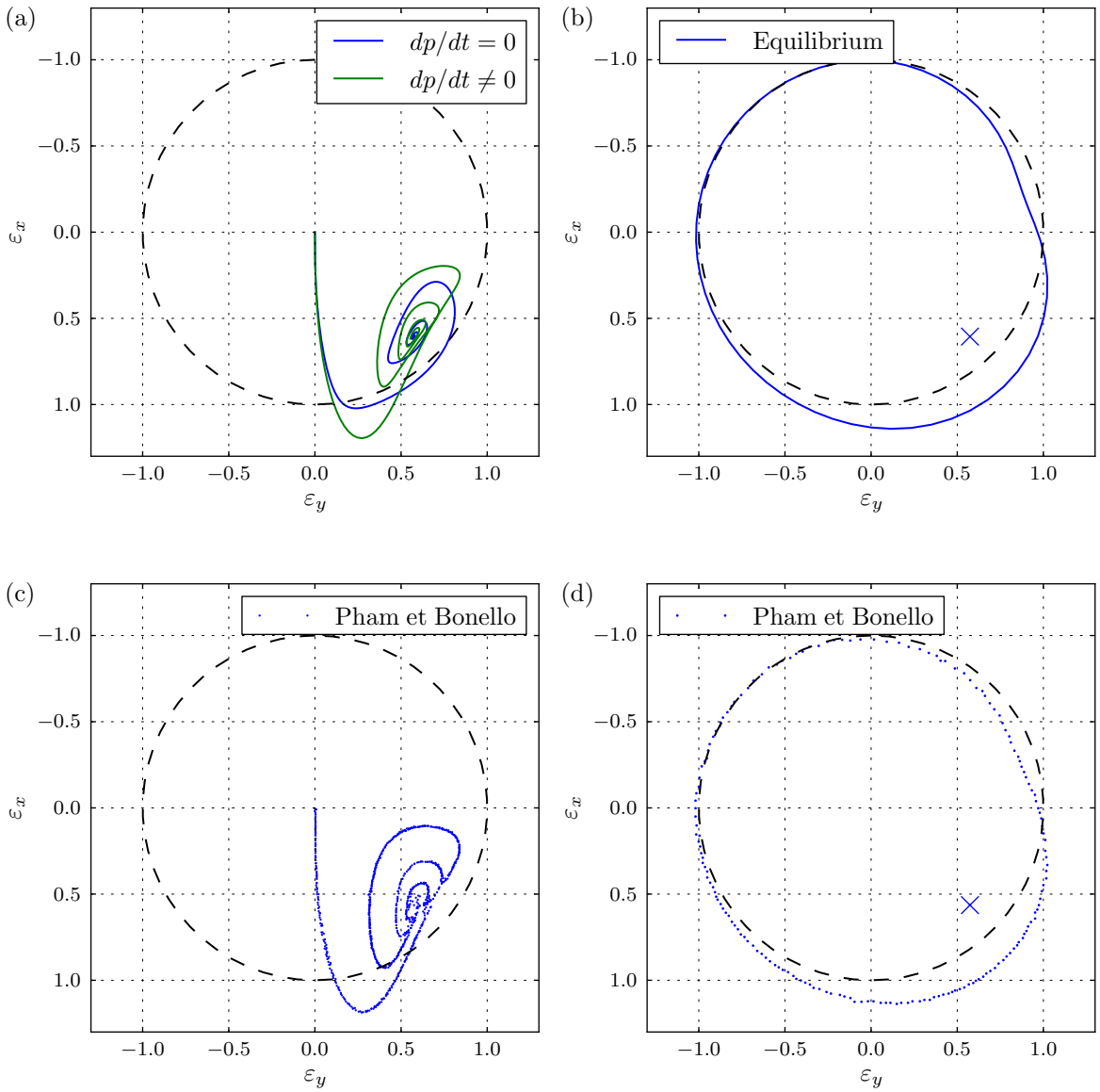

Figure 2: (a) Journal response when dropped from the bearing centre. The dashed line indicates the undeformed foil shape. (b) Deformed and undeformed foil shape at the static equilibrium. (c) and (d) Journal response results and foil deflection extracted from Pham and Bonello [4, 18].

observed, as illustrated in Fig. 6. Not unexpectedly, the synchronous vibrations amplitude grows to approximately twice the size, compared to the previous simulation, which had half the mass unbalance. What is less expected is the fact, that the rotor is now tracing a quasi-periodic orbit and as seen in the associated spectra, four sub-synchronous vibrations appears. With two of them having significant amplitudes at approximately 150 Hz and 195 Hz. Dependent on the general rotor and bearing geometry and the running conditions, these sub-synchronous vibrations can appear with very high amplitudes that can lead to bearing failures. In the simulated example the rotor unbalances are between ISO G2.5 and ISO G16 which are high unbalance levels for a rotor supported by foil bearings. A well designed rotor on foil bearings might be stable and trace an almost circular orbit, when the level of unbalance is within a safe range, usually ISO G2.5, but as shown, unstable when outside. Therefore, rotor balancing should be given great attention when mass-producing turbo machinery supported by AFBs.

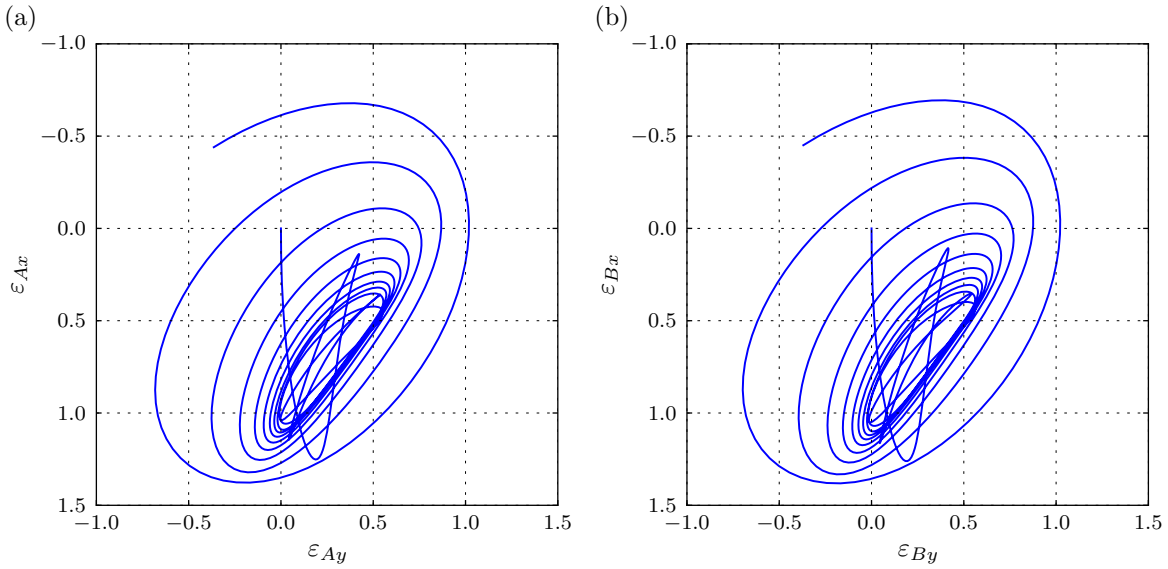

Figure 3: Journal response when dropped from the centre. (a) Bearing A. (b) Bearing B. $\omega = 30,000$ RPM.

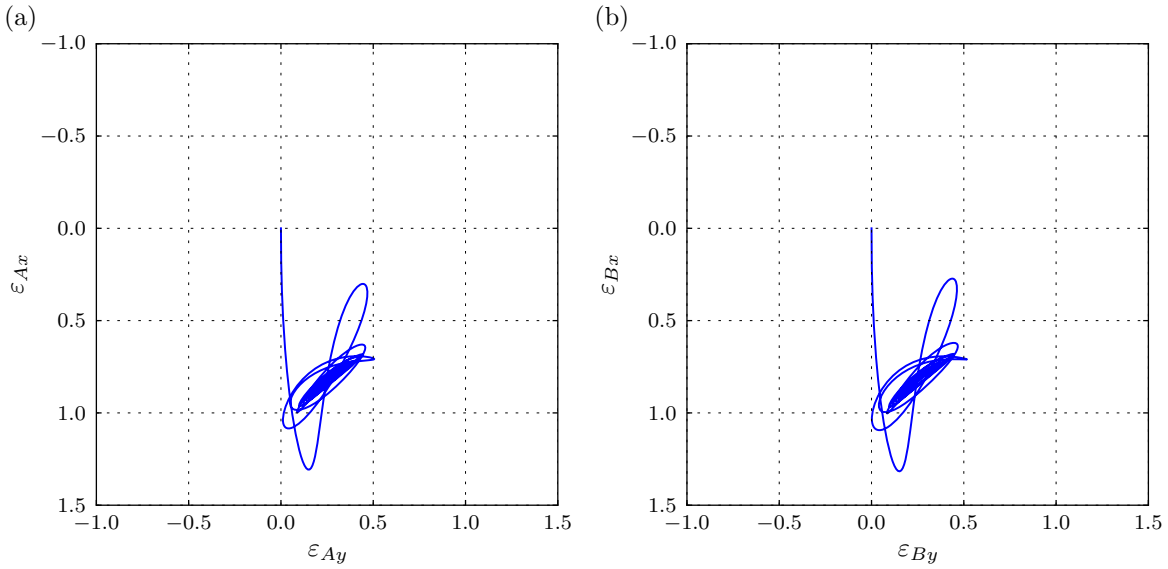

Figure 4: Journal response when dropped from the centre. (a) Bearing A. (b) Bearing B. $\omega = 20,000$ RPM.

4 Conclusion

A method [4, 18] for simulating the rotor response of a rigid rotor supported by AFBs were implemented and validated. The method, which solves for all state variables simultaneously, was compared to calculations in which the time dependent term dp/dt was neglected. The comparison clearly showed that neglecting dp/dt will lead to significant errors, and overestimation of the damping in the bearings.

The influence of rotor mass unbalance, on a rigid shaft supported by two identical AFBs, were investigated as well. This investigation highlighted the importance of balancing turbo machines to a high grade as unbalance can cause sub-synchronous vibrations to occur that can lead to bearing failures.

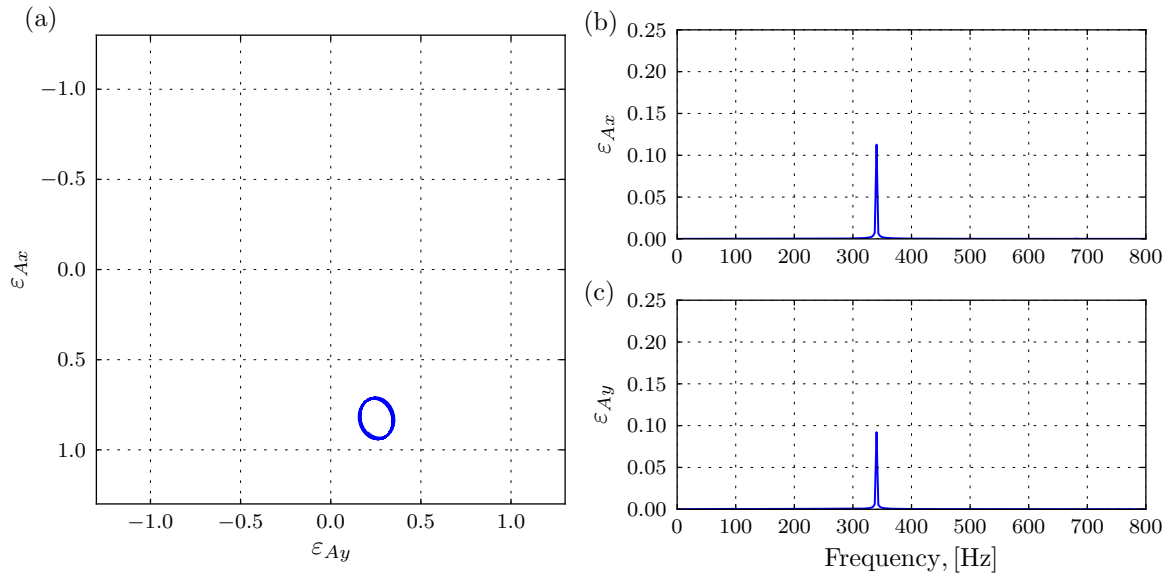

Figure 5: Journal steady state unbalance response after 1.5 s. (a) Bearing A. (b) Bearing B. $\omega = 20,000$ RPM.

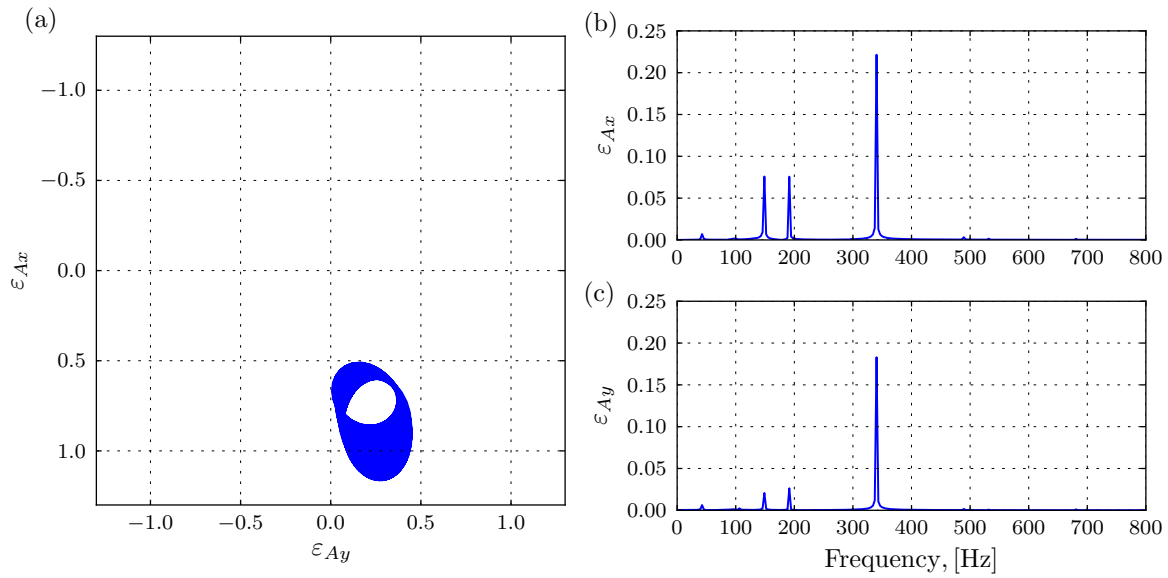

Figure 6: Journal steady state unbalance response after 1.5 s. (a) Bearing A. (b) Bearing B. $\omega = 20,000$ RPM.

A Rotor model matrices

The mass and gyroscopic matrices for a rigid rotor can be written as:

$$[M] = \frac{1}{l^2}\begin{bmatrix} l_2^2 m_x + I_{yy} & 0 & l_1 l_2 m_x - I_{yy} & 0 \\ 0 & l_2^2 m_y + I_{xx} & 0 & l_1 l_2 m_y - I_{xx} \\ l_1 l_2 m_x - I_{yy} & 0 & l_1^2 m_x + I_{yy} & 0 \\ 0 & l_1 l_2 m_y - I_{xx} & 0 & l_1^2 m_y + I_{xx} \end{bmatrix}, \quad [G] = \frac{1}{l^2}\begin{bmatrix} 0 & -I_{zz} & 0 & I_{zz} \\ I_{zz} & 0 & -I_{zz} & 0 \\ 0 & I_{zz} & 0 & -I_{zz} \\ -I_{zz} & 0 & I_{zz} & 0 \end{bmatrix} \tag{20}$$

The non-dimensional form of the mass and gyroscopic matrices and the mass unbalance vector are:

$$[\tilde{G}] = \frac{\omega^2 C}{p_a R^2}[G], \quad [\tilde{M}] = \frac{\omega^2 C}{p_a R^2}[M], \quad \{\tilde{F}_{ub}\} = \begin{Bmatrix} \frac{u_A \omega^2}{p_a R^2} \begin{Bmatrix} \cos(\tau) \\ \sin(\tau) \end{Bmatrix} \\ \frac{u_B \omega^2}{p_a R^2} \begin{Bmatrix} \cos(\tau) \\ \sin(\tau) \end{Bmatrix} \end{Bmatrix}. \tag{21}$$

B Film height

For a segmented journal bearing, with inlet slope and the nomenclature as illustrated in Fig. 1b, the dimensionless rigid film height can be written as:

$$\tilde{h}_r = \begin{cases} 1 + \varepsilon_x \cos(\theta) + \varepsilon_y \sin(\theta) - \tilde{h}_s \frac{\theta - \theta_i}{\theta_s}, & \theta_{li} \le \theta \le \theta_i \\ 1 + \varepsilon_x \cos(\theta) + \varepsilon_y \sin(\theta), & \theta_i < \theta \le \theta_{ti} \end{cases} \tag{22}$$

where

$$\begin{aligned} \theta_i &= \theta_s + \theta_l + \frac{2\pi}{N_p}(i-1) \\ \theta_{li} &= \theta_l + \frac{2\pi}{N_p}(i-1) \\ \theta_{ti} &= \theta_t + \frac{2\pi}{N_p}(i-1) \end{aligned} \tag{23}$$

Discarding the mass of the foil structure, the equation of motion for the foil structure is:

$$\tilde{p} - 1 = \tilde{k}\tilde{h}_c + \tilde{b}\dot{\tilde{h}}_c \quad \text{or} \quad \tilde{h}_c(\tilde{p}, \dot{\tilde{h}}_c) = \frac{\tilde{p} - 1 - \tilde{b}\dot{\tilde{h}}_c}{\tilde{k}} \tag{24}$$

Introducing the mechanical loss factor

$$\eta = \frac{b\omega_s}{k} = \frac{\tilde{b}}{\tilde{k}}\frac{\omega_s}{\omega} \tag{25}$$

Inserting the loss factor into the foil equation of motion yields the first order ordinary differential equation:

$$\dot{\tilde{h}}_c = \left(\frac{\tilde{p} - 1}{\tilde{k}} - \tilde{h}_c\right)\frac{1}{\eta} \tag{26}$$

with $\omega_s/\omega = 1$ meaning the the vibrations in the foil are assumed synchronous.

REFERENCES

[1] E. Anderson, Z. Bai, C. Bischof, S. Blackford, J. Demmel, J. Dongarra, J. Du Croz, A. Greenbaum, S. Hammarling, A. McKenney, and D. Sorensen. *LAPACK Users' Guide*. Society for Industrial and Applied Mathematics, Philadelphia, PA, third edition, 1999.

[2] M. Arghir, S. Le Lez, and J. Frene. Finite-volume solution of the compressible reynolds equation: linear and non-linear analysis of gas bearings. *Proceedings of the Institution of Mechanical Engineers, Part J: Journal of Engineering Tribology*, 220(7):617–627, jan 2006.

[3] J. S. Ausman. An improved analytical solution for self-acting, gas-lubricated journal bearings of finite length. *Journal of Basic Engineering*, 83(2):188–192, 1961.

[4] P. Bonello and H. M. Pham. The efficient computation of the nonlinear dynamic response of a foil–air bearing rotor system. *Journal of Sound and Vibration*, 333(15):3459–3478, 2014.
[5] R. D. Cook, D. S. Malkus, M. E. Plesha, and J. W. Witt. *Concepts and applications of finite element analysis*. John Wiley, New York, 4 edition, 2002.
[6] B. J. Hamrock. *Fundamentals of Fluid Film Lubrication*. McGRAW-HILL Series in Mechanical Engineering. McGRAW-HILL, Inc., New York, 1994.
[7] W. J. Harrison. The hydrodynamical theory of lubrication with special reference to air as a lubricant. *Transactions Cambridge Philosophical Society*, 22:34–54, 1913.
[8] H. Heshmat, J. A. Walowit, and O. Pinkus. Analysis of gas lubricated compliant thrust bearings. *Journal of Lubrication Technology*, 105(4):638–646, 1983.
[9] H. Heshmat, J. A. Walowit, and O. Pinkus. Analysis of gas-lubricated foil journal bearings. *Journal of Lubrication Technology*, 105(4):647–655, 1983.
[10] A. C. Hindmarsh. Odepack, a systematized collection of ode solvers, stepleman rs, scientific computing, 55-64, 1983.
[11] J. S. Larsen, A. J.-T. Hansen, and I. F. Santos. Experimental and theoretical analysis of a rigid rotor supported by air foil bearings. *Mechanics & Industry*, 2014.
[12] J. S. Larsen and I. F. Santos. Efficient solution of the non-linear reynolds equation for compressible fluid using the finite element method. *Journal of the Brazilian Society of Mechanical Sciences and Engineering*, pages 1–13, 2014.
[13] J. S. Larsen, A. C. Varela, and I. F. Santos. Numerical and experimental investigation of bump foil mechanical behaviour. *Tribology International*, 74(Complete):46–56, 2014.
[14] S. Le Lez, M. Arghir, and J. Frêne. Nonlinear numerical prediction of gas foil bearing stability and unbalanced response. *Journal of Engineering for Gas Turbines and Power*, 131(1):012503, 2009.
[15] D. Lee, Y.-C. Kim, and K.-W. Kim. The dynamic performance analysis of foil journal bearings considering coulomb friction: Rotating unbalance response. *Tribology Transactions*, 52(2):146–156, 2009.
[16] J. W. Lund. Calculation of stiffness and damping properties of gas bearings. *Journal of Lubrication Technology*, pages 793–804, 1968.
[17] J. B. Olsen. Nonlinear dynamic behavior of rigid rotor foil bearing system. Master's thesis, Technical University of Denmark, 2014.
[18] H. M. Pham and P. Bonello. Efficient techniques for the computation of the nonlinear dynamics of a foil-air bearing rotor system. In *ASME Turbo Expo 2013: Turbine Technical Conference and Exposition*, pages –07, 2013.
[19] J.-H. Song and D. Kim. Foil gas bearing with compression springs: Analyses and experiments. *ASME Journal of Tribology*, 129(3):628–639, 2007.
[20] B. Sternlicht and R. C. Elwell. Theoretical and experimental analysis of hydrodynamic gas-lubricated journal bearings. *American Society of Mechanical Engineers – Papers*, (57), 1957.
[21] V. Stingelin. *Theoretische und experimentelle Untersuchungen an Gaslagern*. PhD thesis, Eidgenössischen Technischen Hochschule in Zürich, 1963.
[22] C.-C. Wang and C.-K. Chen. Bifurcation analysis of self-acting gas journal bearings. *Journal of Tribology*, 123(4):755, 2001.
[23] J. Zhang, W. Kang, and Y. Liu. Numerical method and bifurcation analysis of jeffcott rotor system supported in gas journal bearings. *Journal of Computational and Nonlinear Dynamics*, 4(1):011007, 2009.